Physicochem. Probl. Miner. Process., 62(5), 2026, 230979

http://www.journalssystem.com/ppmp

Physicochemical Problems of Mineral Processing

ISSN 1643-1049

Characterization of manganoferrous (Fe-Mn) oxide ore from Türkiye-Şırnak region

A. Ufuk Deniz [1], Arman Ehsani [1], Fatih Çavuşlu [2], Ilhan Ehsani [3]

[1] Adana Alparslan Türkeş Science and Technology University, Faculty of Engineering, Department of Mining Engineering, 01250, Adana, Türkiye

[2] Adana Alparslan Türkeş Science and Technology University, Faculty of Engineering, Department of Materials Science and Engineering, 01250, Adana, Türkiye

[3] Şırnak University, Faculty of Engineering, Department of Mining Engineering, 73000, Şırnak, Türkiye

Corresponding author: aehsani@atu.edu.tr (Arman Ehsani)

Abstract: Manganoferrous (Fe-Mn) oxide ores represent important mineral resources owing to their applications in metallurgical industries and their growing significance as potential sources of critical raw materials. In this study, a manganoferrous (Fe-Mn) oxide ore collected from the Şırnak region of southeastern Türkiye was comprehensively characterized using X-ray diffraction (XRD), X-ray fluorescence spectroscopy (XRF), scanning electron microscopy coupled with energy-dispersive spectroscopy (SEM-EDS), elemental mapping, Fourier-transform infrared spectroscopy (FT-IR), and thermogravimetric–differential thermal analysis (TG-DTA-DTG). XRD analysis identified quartz (SiO_2), goethite [FeO(OH)], and bixbyite [$(Fe,Mn)_2O_3$] as the major mineral phases present in the ore. XRF results revealed that the sample contains approximately 49.3 wt.% Fe_2O_3, 14.6 wt.% MnO, and 18.6 wt.% SiO_2, indicating a manganoferrous (Fe-Mn) oxide ore or sub/low-grade ferruginous manganese ore characterized by significant iron enrichment and moderate manganese content. SEM-EDS and elemental mapping analyses demonstrated heterogeneous mineral distribution and a strong spatial association between iron and manganese oxide phases. FT-IR spectroscopy confirmed the occurrence of hydroxyl-bearing iron oxyhydroxides, mixed Fe-Mn oxide minerals, and silicate gangue through characteristic O–H, Fe–O, Mn–O, and Si–O vibrational bands. TG-DTA-DTG analysis revealed multi-stage thermal decomposition behavior with an overall mass loss of approximately 11.9 wt.%, primarily attributed to dehydration and dehydroxylation reactions associated with goethite-bearing phases. The findings provide valuable mineralogical and thermal information for future beneficiation, reduction roasting, magnetic separation, and hydrometallurgical processing studies involving ferruginous manganese ores from southeastern Türkiye.

Keywords: iron-manganese ore, mineralogy, characterization, bixbyite, FTIR, TG-DTA-DTG

1. Introduction

Manganese (Mn), a 7th group element of the periodic table, is the twelfth most abundant element in the Earth's crust with a molecular weight of 54.93 and a melting point of 1244 °C (Çardaklı, 2010; Singh et al., 2020). It is one of the most strategically important transition metals used in modern industry due to its extensive applications in metallurgical, chemical, energy-storage, and advanced material technologies. Globally, approximately 90–95% of manganese consumption is associated with the iron and steel industry, where manganese acts as a deoxidizing, desulfurizing, and alloy-strengthening agent. The addition of manganese significantly improves the hardness, wear resistance, tensile strength, and impact resistance of steel products, making it indispensable for structural steels, stainless steels, rail steels, and high-strength low-alloy steels (Yi et al., 2017; U.S. Geological Survey, 2021).

In addition to traditional metallurgical applications, manganese has gained increasing strategic importance in recent decades because of its use in lithium-ion batteries, rechargeable cathode systems, renewable energy storage technologies, and electric vehicle production. Particularly, manganese-rich

DOI: 10.37190/ppmp/230979

cathode chemistries such as lithium manganese oxide (LMO) and nickel-manganese-cobalt (NMC) systems have attracted significant attention due to their comparatively low cost, high thermal stability, and favorable electrochemical performance (Li et al., 2021). Iron (Fe), another industrially essential transition metal, frequently occurs together with manganese in natural ore systems. However, the coexistence of Fe- and Mn-bearing minerals creates substantial challenges during beneficiation and metallurgical processing because these elements often exhibit similar physicochemical properties, magnetic behavior, density characteristics, and mineral associations. Consequently, the selective separation and enrichment of manganese from ferruginous ore systems remain technically complex and economically demanding (Ringdalen et al., 2021). The mineralogical complexity of Fe-Mn oxide ores becomes even more problematic in low-grade deposits, where manganese minerals are finely disseminated within silicate or iron-rich gangue matrices.

Manganese ores are commonly classified according to their manganese grade and mineralogical composition, i.e., Mn content. High-grade manganese ores generally contain more than 44% Mn, medium-grade ores contain between 35% and 44% Mn, whereas low-grade ores contain less than 35% Mn (Gao et al., 2012). According to the classification proposed by the U.S. Bureau of Mines, ores containing more than 35% Mn are classified as manganese ores, those containing 10–35% Mn are termed ferruginous manganese ores, while ores containing 5–10% Mn are categorized as manganoferous (Fe-Mn) iron ores (or sub/low-grade ferruginous manganese ores) (State Planning Organization (DPT), 2001; Christie, 2007; Çardaklı, 2010). In addition, manganese ores are also classified as metallurgical, battery, and chemical grades based on their application and quality. Metallurgical grade ores are used in ferromanganese or special manganese alloy production or as chemicals. Battery grade ores, which can be of natural or synthetic origin, consist of manganese oxides with varying degrees of purity. Chemical quality manganese ores are classified as group A or group B depending on their manganese, iron and silica contents (Çardaklı, 2010). Despite their relatively low manganese content, ferruginous and manganoferous ores are increasingly becoming economically relevant due to the depletion of high-grade deposits worldwide and the rapidly growing demand for manganese in advanced industrial technologies (Singh et al., 2020).

The global decline of easily accessible high-grade manganese resources has led researchers and mining industries to focus increasingly on the characterization, beneficiation, and utilization of low-grade manganese-bearing ores. In many countries, low-grade ferruginous manganese ores represent large untapped resources that require advanced mineralogical understanding and efficient beneficiation strategies for economic utilization. Therefore, detailed mineralogical and chemical characterization studies have become essential preliminary steps before developing suitable beneficiation flowsheets and metallurgical extraction processes (Liu et al., 2024).

The mineralogy of Fe-Mn deposits is highly variable and may include oxide, hydroxide, carbonate, and silicate phases. Common manganese-bearing minerals include pyrolusite (MnO_2), psilomelane ($BaMn_9O_{16}(OH)_4$), braunite ($Mn_2Mn_6SiO_{12}$), bixbyite ($Mn_2Fe_2O_3$), hausmannite (Mn_3O_4), manganite ($Mn_2O_3H_2O$), rhodochrosite ($MnCO_3$), and jacobsite (Fe_2MnO_4), whereas iron typically occurs as hematite (Fe_2O_3), goethite (FeOOH), magnetite (Fe_3O_4), limonite (FeOOH-nH_2O), or siderite ($FeCO_3$) (Singh et al., 2020). Among these minerals, bixbyite [$(Mn, Fe)_2O_3$] is particularly important because it represents a mixed Fe-Mn oxide phase that reflects complex geological formation conditions and may significantly influence beneficiation behavior. The coexistence of bixbyite with goethite and quartz in the ore sample investigated in this study often indicates hydrothermal or sedimentary remobilization processes involving oxidation and secondary enrichment (Maynard, 1983; Yan et al., 2022).

The geological formation of manganese deposits is associated with several genetic environments, including sedimentary, hydrothermal, supergene, volcanic-sedimentary, and lateritic processes (Li and Xu, 2024). Sedimentary manganese deposits are generally formed through chemical precipitation under marine or lacustrine conditions, whereas hydrothermal deposits are commonly related to volcanic activity and fluid circulation systems. Lateritic manganese deposits form through intense weathering and supergene enrichment processes under tropical climatic conditions. In many cases, iron and manganese mineralization coexist due to similar geochemical mobility during oxidation-reduction reactions and hydrothermal alteration (Xiao et al., 2019; Elmi et al., 2023).

Türkiye possesses significant mineral diversity due to its complex tectonic and geological evolution (Şaşmaz et al., 2014; Öztürk et al., 2019; Boztas et al., 2025). Several regions in eastern and southeastern

Türkiye host economically important Fe-Mn mineralizations associated with ophiolitic complexes, volcanic-sedimentary units, hydrothermal systems, and metamorphic sequences. Previous studies conducted in the Elazığ–Malatya region reported the occurrence of braunite, bixbyite, jacobsite, pyrolusite, manganite, and psilomelane as major manganese-bearing phases within ferromanganese deposits (Şaşmaz et al., 2014). Similarly, manganese mineralization in the Battalgazi–Malatya region was reported to occur within siliceous and clay-rich sedimentary units, accompanied by quartz and iron oxides (Yapici and Bahçeli, 2012).

Southeastern Türkiye, including Şırnak province, represents a geologically complex region characterized by extensive tectonic activity, sedimentary basin evolution, metamorphism, and hydrothermal alteration processes. These geological processes have contributed to the formation, remobilization, and enrichment of various metallic and industrial mineral deposits including Fe, Mn, Cu, Zn, Pb, Cr, phosphate, and clay minerals (Imamoğlu, 2005; Şaşmaz et al., 2014). Despite the mineralogical importance of this region, relatively limited scientific studies have focused specifically on the detailed characterization of Fe-Mn oxide ores from Şırnak province. Therefore, comprehensive mineralogical and chemical investigations are necessary to understand better the composition, mineral associations, and beneficiation potential of these ore systems. As a whole, Eastern and southeastern Türkiye host diverse Fe–Mn deposits linked to ophiolites, volcanic–sedimentary successions, and hydrothermal systems. Research from nearby regions helps frame the geological setting, mineralogy, and likely genesis of Şırnak-type Fe–Mn oxide ores, while highlighting how little is known specifically for Şırnak.

Ore characterization studies constitute one of the most critical stages of mineral processing and extractive metallurgy research. Modern characterization techniques such as X-ray diffraction (XRD), X-ray fluorescence (XRF), scanning electron microscopy coupled with energy-dispersive spectroscopy (SEM-EDS), elemental mapping, Fourier transform infrared spectroscopy (FTIR), and Thermogravimetry combined with Differential Thermal Analysis (TG-DTA-DTG) provide valuable information regarding crystalline phases, elemental composition, grain morphology, mineral liberation characteristics, thermal behavior, and textural relationships. Such information is essential for designing efficient beneficiation methods including magnetic separation, flotation, gravity concentration, selective reduction roasting, hydrometallurgical extraction, and pyrometallurgical treatment (Lotter et al., 2011; Schouwstra and Smit, 2011; Poojari et al., 2024).

X-ray diffraction (XRD) analysis is particularly useful for identifying crystalline mineral phases and determining the dominant oxide and gangue minerals present within ore systems. XRF analysis provides quantitative elemental and oxide compositions, enabling ore classification and preliminary economic assessment. SEM-EDS and mapping analyses allow detailed examination of particle morphology, mineral textures, elemental distributions, and intergrowth relationships between valuable minerals and gangue phases. Complementing these techniques, Fourier-transform infrared spectroscopy (FT-IR) facilitates the functional group tracking of amorphous components and hydrous minerals, while thermogravimetric and differential thermal analysis (TG-DTA-DTG) evaluate structural dehydroxylation, carbonate decomposition, and phase transformations of iron-manganese minerals during heating (Ali et al., 2023). The integration of these analytical techniques significantly improves the understanding of complex Fe-Mn ore systems. It supports the development of suitable beneficiation strategies, particularly in predicting high-temperature roasting behaviors and mineral reduction kinetics (Safarov et al., 2025).

In recent years, increasing attention has also been directed toward sustainable and environmentally responsible mineral processing approaches for low-grade ores. Since high-grade manganese resources are gradually decreasing worldwide, the beneficiation and utilization of manganoferrous (Fe-Mn)/low- to sub-grade ferruginous manganese ores have become increasingly important from both economic and strategic perspectives. Moreover, the growing demand for manganese in electric vehicle batteries and renewable energy technologies further increases the importance of identifying alternative manganese resources and improving ore beneficiation technologies (Naseri et al., 2026).

Although ferruginous manganese deposits have been reported from different regions of Türkiye (Öztürk et al., 2019; Şaşmaz et al., 2014), detailed multi-technique characterization studies focusing on the Şırnak manganoferrous Fe–Mn oxide ore remain scarce. The limited availability of integrated

mineralogical, chemical, microstructural, and thermal data restricts a comprehensive understanding of the ore and complicates the selection of appropriate beneficiation and metallurgical processing routes (Bhoja et al., 2021). This study addresses this gap by combining complementary characterization techniques to establish a comprehensive physicochemical database for the investigated ore.

Therefore, the primary objective of this study is to provide a comprehensive characterization of the investigated manganoferrous Fe-Mn oxide ore and evaluate its mineralogical uniqueness, beneficiation potential, and possible industrial significance. Prior to analytical investigations, the ore sample underwent standard comminution and homogenization procedures to ensure representative and reliable characterization results. XRD, XRF, SEM-EDS, elemental mapping, FT-IR, and TG-DTA-DTG analyses were systematically conducted to determine and evaluate the mineralogical phases, elemental composition, grain morphology, elemental distributions, functional groups and bonds, and phase transformations within the ore sample. By integrating these complementary techniques, this study contributes to the limited knowledge of Fe–Mn mineralization in southeastern Türkiye. It provides a valuable foundation for future beneficiation, liberation, hydrometallurgical, and pyrometallurgical investigations of similar manganoferrous and sub/low-grade ferruginous manganese ores.

2. Materials and methods

2.1. Materials

Fe-Mn oxide ore was collected from the Şırnak region located in southeastern Türkiye (Fig. 1-a). The collected sample was initially crushed and subsequently ground to a particle size below 500 μm using a laboratory-scale ball mill. The ground material was homogenized and prepared for mineralogical, chemical, spectroscopic, and thermal characterization analyses (Fig. 1-b).

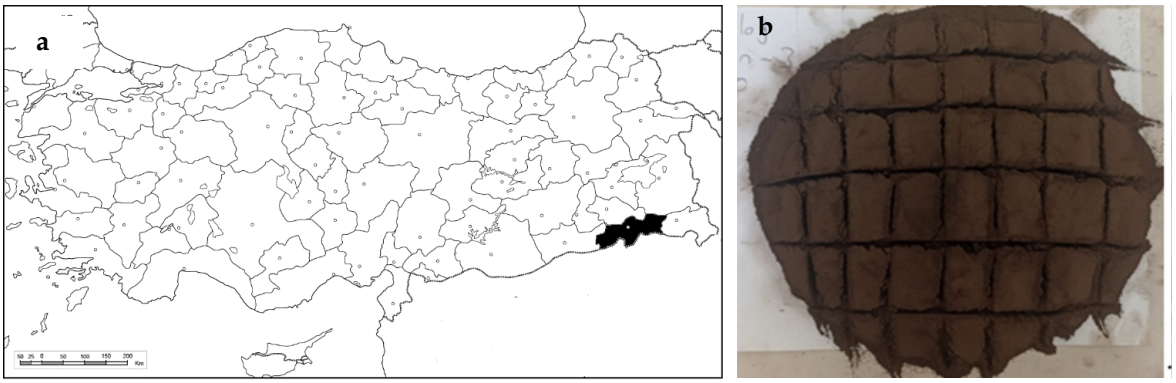

Fig. 1. (a) Şırnak Province in Southeastern Türkiye-black painted region) and b) ground ore sample

In order to prepare samples for XRF, XRD, SEM, FT-IR, and TG-DTA-DTG analyses, the representative ground samples (obtained by sampling methods: coning and quartering method, grid-based sampling) were further finely ground using an agate mortar grinder (Retsch RM200, Germany) for 15 minutes. This procedure ensured that the particle size and sample uniformity were appropriate for accurate instrumental analysis. Following this fine grinding step, a grid-based sampling method was applied to ensure representative sample selection for XRD, XRF, SEM-EDS, FT-IR, and TG-DTA-DTG analysis. The powdered sample was evenly spread on a clean flat surface, and equal-sized amounts were systematically collected from across a marked grid. This method ensured a representative cross-section of the entire sample.

2.2. Methods

The particle size distribution of the crushed and ground ore sample was determined using a standard sieve analysis in accordance with ASTM standards (ASTM E11/E11M-20). X-ray diffraction (XRD) analysis was conducted to identify the crystalline phases (i.e., minerals) present in the ore samples. The analysis was performed using a Rigaku MiniFlex 600 diffractometer (Japan), equipped with Cu-Kα radiation (λ = 1.5406 Å) operating at a tube voltage of 40 kV and a current of 15 mA. Measurements

were carried out in θ/2θ mode under the following conditions: scan range: 5°–65° (2θ); scan speed: 2°/min, and step size: 0.02°. Mineral phases were identified by comparison with standard reference patterns available in the Crystallography Open Database (COD/DB number) database. Also, the crystallite sizes of the identified mineral phases were estimated using the Scherrer equation (Eq. 1, (Cullity, 1956)) based on the full width at half maximum (FWHM) values of selected XRD reflections:

$$D = K\lambda / (\beta \cos \theta) \quad (1)$$

where D is the crystallite size, K is the Scherrer constant (has been taken as 0.94), λ is the X-ray wavelength (Å; has been taken as 1.5418 Å), β is the peak width at half maximum (FWHM in radians), and θ is the Bragg diffraction angle (°). The calculated crystallite sizes were used to evaluate the crystallinity and microstructural characteristics of the identified mineral phases.

The chemical composition of the powdered ore samples was determined using a Rigaku ZSX Primus II wavelength-dispersive X-ray fluorescence (WDXRF) spectrometer (Japan). The analysis was conducted on pressed powder samples without a binder. The obtained chemical data were used to support the mineralogical interpretation derived from XRD analysis.

Scanning Electron Microscopy (SEM) analysis was performed using an FEI Quanta FEG 650 (USA) microscope at the Central Laboratory of Çukurova University. The instrument is equipped with EDS and mapping capabilities, allowing for microstructural and elemental characterization of the samples. Prior to analysis, samples were coated with a conductive layer. Elemental mapping analyses were additionally performed to evaluate the spatial distribution and association of Fe, Mn, Si, O, and other major elements within the ore matrix.

Fourier-transform infrared spectroscopy (FT-IR) analysis was performed to identify the functional groups, hydroxyl-bearing phases, and characteristic vibrational modes of the minerals present in the investigated Fe-Mn oxide ore. The FT-IR spectrum was recorded using a JASCO FT/IR-6700 Fourier-transform infrared spectrometer (JASCO Corporation, Japan) equipped with an Attenuated Total Reflectance (ATR) accessory. Spectral measurements were conducted over the wavenumber range of 4000–400 cm^{-1}. The FT-IR results were subsequently used as complementary evidence to support the mineralogical interpretations derived from XRD, SEM-EDS, elemental mapping, and thermal analysis results.

Thermogravimetric (TG), differential thermal (DTA), and derivative thermogravimetric analysis (DTG) were conducted to investigate the thermal stability, dehydration behavior, phase transformations, and decomposition characteristics of the investigated Fe-Mn oxide ore. Thermal analyses were performed using a Mettler Toledo TGA/DSC 3+ thermal analysis system (Mettler Toledo, Switzerland). A representative ore sample was subjected to thermal analysis over the temperature range of 25–1200 °C. The obtained thermal analysis results were interpreted together with the mineralogical and spectroscopic findings derived from XRD, FT-IR, SEM-EDS, and elemental mapping analyses. Particular attention was given to the thermal behavior of hydroxyl-bearing iron oxyhydroxides, mixed Fe-Mn oxide phases, and silicate minerals. The TG-DTA-DTG data provided valuable information regarding the thermal stability of the ore and its potential suitability for thermal beneficiation, reduction roasting, and subsequent metallurgical processing applications.

3. Results and discussion

3.1. Particle size distribution

Particle size distribution plays a critical role in mineral processing because it directly influences mineral liberation, separation efficiency, reagent consumption, grinding energy requirements, and downstream beneficiation performance. The comminution behavior of Fe-Mn oxide ores is particularly important because manganese-bearing minerals are frequently interlocked with iron oxides and siliceous gangue phases. Therefore, understanding the particle size characteristics of the ground ore sample is essential for evaluating the suitability of the material for future beneficiation studies.

The sieve analysis results (Fig. 2) demonstrated that the ore sample exhibits a relatively broad yet controlled particle size distribution after crushing and grinding operations. The determined d_{25}, d_{50}, and d_{80} values were approximately 92 μm, 141 μm, and 341 μm, respectively. These values indicate that the

comminution process produced a sufficiently fine particle size range suitable for mineralogical characterization and preliminary beneficiation studies.

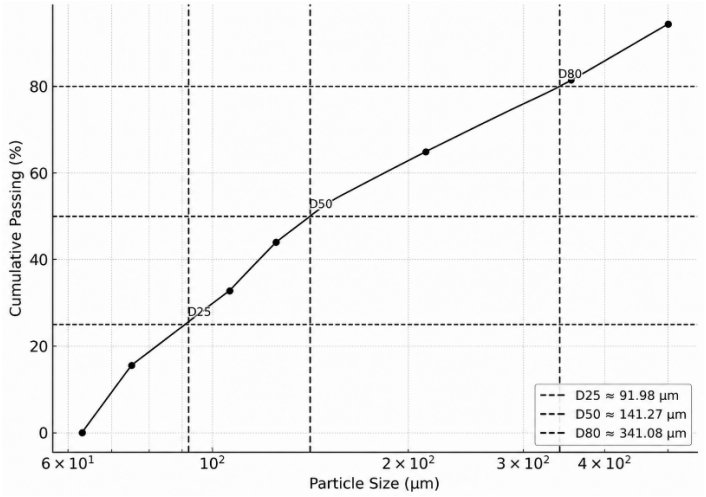

Fig. 2. Particle size distribution of the ore sample

The relatively smooth cumulative distribution curve also indicates that the ore sample underwent effective and homogeneous grinding without excessive generation of ultra-fine particles. Excessive slime formation during grinding can negatively affect the efficiency and selectivity of benefication processes, such as flotation, magnetic separation, and solid-liquid separation (thickening). Therefore, the observed particle size profile may provide favorable conditions for future beneficiation investigations.

3.2. X-ray diffraction (XRD) analysis

X-ray diffraction (XRD) analysis was conducted to identify the crystalline phases present in the ore sample (Fig. 3). The resulting diffraction pattern displayed several distinct peaks, notably at 21.28°, 26.68°, 33.14°, 36.63°, and 50.20°.

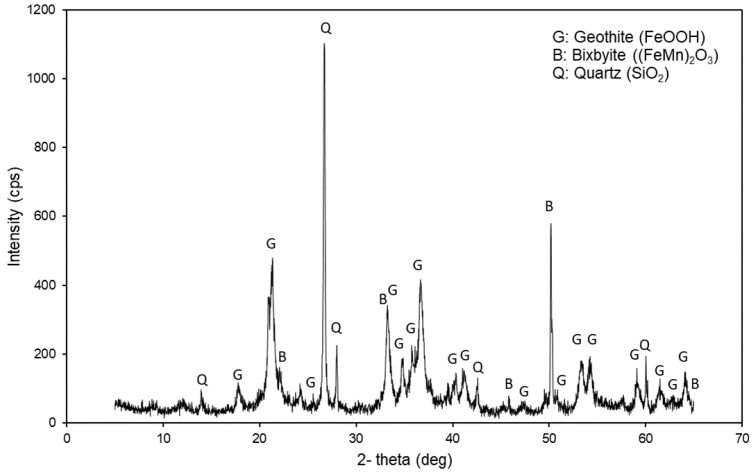

Fig. 3. XRD pattern of the ore sample

The most intense peak at 26.68° is characteristic of quartz (SiO_2), which is commonly found in siliceous matrices. The silica (quartz) is one of the main gangue minerals in low-grade Fe-Mn ores (Ismail et al., 2016; Niyonzima et al., 2021). The peaks near 36.63° and 21.28° are attributed to goethite (FeO-OH), reflecting the iron content of the sample. The presence of these minerals indicates that the investigated ore belongs to a manganoferrous (Fe-Mn) or sub/low-grade ferruginous manganese oxide system with significant siliceous gangue content. Furthermore, the main Mn-bearing minerals are often

intergrown with Fe oxides, a characteristic feature commonly reported for ferruginous manganese ores (Ismail et al., 2016; Niyonzima et al., 2021; Moustafa et al., 2024).

The peak observed at 50.20° is associated with bixbyite $(Fe\text{-}Mn)_2O_3$, a manganese-iron oxide, indicating the presence of manganese-bearing phases. Bixbyite is a mixed iron-manganese oxide mineral that may form under oxidizing conditions and is frequently associated with hydrothermal or metamorphically altered manganese deposits. The occurrence of bixbyite is mineralogically significant because it confirms the coexistence of Fe and Mn within the same oxide structure.

The identification of bixbyite may also have important implications for beneficiation behavior. Since Fe and Mn coexist within the same crystal structure, conventional physical separation methods may exhibit limited selectivity unless sufficient mineral liberation is achieved. Furthermore, the intimate association between iron and manganese phases may require selective reduction roasting, magnetic separation, or hydrometallurgical treatment to improve manganese recovery (Yi et al., 2017; Niyonzima et al., 2021). In addition, the coexistence of quartz, goethite, and bixbyite indicates that the ore sample exhibits a complex mineralogical structure involving oxide and silicate phases. Similar mineral assemblages have previously been reported in ferruginous manganese deposits from Türkiye, India, China, and several African manganese provinces (Şaşmaz et al., 2014).

The obtained mineralogical results also indicate that the ore is relatively low-grade in terms of manganese content but may still possess considerable scientific and economic importance because of its unique Fe-Mn oxide associations. The identification of bixbyite, in particular, provides valuable information regarding the genesis and alteration history of the deposit (Elmi et al., 2023).

3.3. X-ray fluorescence (XRF) analysis

The chemical composition of the ore was determined by X-ray fluorescence (XRF) analysis, which revealed that the sample is dominated by iron and manganese oxides, accompanied by a moderate amount of silicate gangue (Table 1). Elemental results show that Fe and Mn are present at 29.7% and 9.77%, respectively.

Table 1. XRF analysis (major phases and elements) of the ore sample

Component	**Fe_2O_3**	**MnO**	**SiO_2**	**Al_2O_3**	**CaO**
Content (wt.%)	49.3	14.6	18.6	4.14	0.769
Element	Fe	Mn	Si	Al	Na_2O
Content (wt.%)	29.7	9.77	7.91	2.00	0.544

The XRF analysis results revealed that the ore sample is predominantly composed of Fe_2O_3 (49.3 wt.%) and MnO (14.6 wt.%), accompanied by significant amounts of SiO_2 (18.6 wt.%) and smaller quantities of Al_2O_3, CaO, Na_2O, and other minor oxides.

The high Fe_2O_3 content indicates that the investigated sample belongs primarily to a ferruginous ore system. Meanwhile, the MnO concentration confirms the presence of economically relevant manganese mineralization despite the relatively low overall manganese grade. According to conventional ore classification systems (State Planning Organization (DPT), 2001; Christie, 2007; Çardaklı, 2010), the investigated sample can be categorized as a sub/low-grade ferruginous manganese ore or manganoferrous iron ore.

The silica content (18.6% SiO_2) indicates that quartz and silicate gangue minerals constitute a major portion of the ore matrix. High silica content is generally considered undesirable in metallurgical processing because it may increase slag volume, flux consumption, and energy requirements during smelting operations. However, from a mineral processing perspective, quartz gangue may potentially be removed through suitable physical beneficiation methods if adequate mineral liberation can be achieved.

The relatively low concentrations of CaO, MgO, TiO_2, sulfur, zinc, and lead (all below %1) suggest that the ore does not contain excessively high levels of deleterious impurities. This may represent an advantage for future beneficiation and metallurgical processing studies.

In addition, the chemical composition suggests that the investigated ore may potentially be suitable for further beneficiation studies involving gravity concentration, magnetic separation, reduction

roasting, or hydrometallurgical extraction techniques. However, detailed liberation analysis and beneficiation testing would be necessary before evaluating the economic feasibility of such processes. The obtained XRF results are generally consistent with the XRD findings, where goethite, bixbyite, and quartz were identified as the dominant mineral phases. The strong correlation between mineralogical and chemical analyses increases the reliability of the characterization results.

3.4. SEM- EDS- mapping analysis

SEM investigations revealed that the ore sample consists predominantly of angular, fractured, and relatively coarse particles with heterogeneous surface textures (Fig. 4). At lower magnifications, the particles exhibit irregular morphologies and rough surfaces. In contrast, higher magnification images revealed the presence of finer secondary phases attached to larger grains.

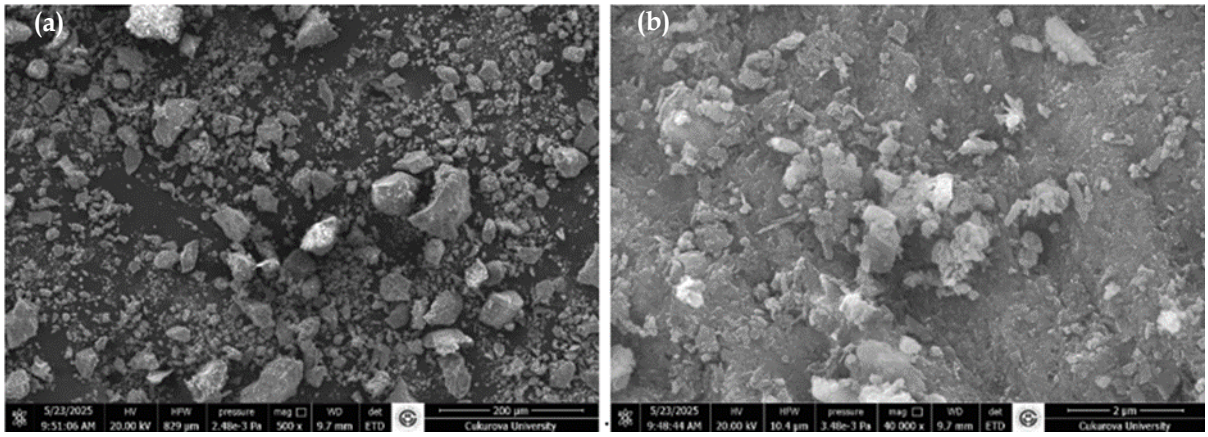

Fig. 4. SEM analysis of the ore sample (a) Mag ×500; (b) Mag ×40000)

The angular morphology of the particles suggests brittle fracture behavior during comminution. Such fracture characteristics are commonly observed in oxide-rich ore systems containing quartz and iron oxides. The fractured surfaces and porous textures observed in some particles may improve reagent penetration during hydrometallurgical leaching processes (Ghadiri et al, 2020).

The heterogeneous grain morphology observed in the SEM images also indicates that the ore contains multiple mineral phases with varying mechanical properties. Quartz-rich particles generally exhibit more brittle fracture behavior, whereas iron oxy-hydroxide phases such as goethite may display relatively porous and earthy textures (Ali et al., 2016; Sobouti et al., 2020).

The SEM observations further suggest that the investigated ore may exhibit partial mineral liberation after grinding. However, certain particles still appear to contain composite intergrowths between oxide and silicate phases. This observation is particularly important because incomplete liberation may reduce the efficiency of physical separation techniques such as magnetic separation or flotation (Semsari Parapari et al., 2022).

The presence of fine secondary phases adhering to larger particles may additionally indicate secondary oxidation, weathering, or alteration processes. Similar textural features have previously been reported in weathered ferruginous manganese ores subjected to hydrothermal alteration and supergene enrichment.

EDS analysis confirmed that oxygen, iron, manganese, silicon, and aluminum constitute the dominant elements within the investigated sample (Fig. 5). The high oxygen content is consistent with the oxide and oxyhydroxide nature of the identified mineral phases. The strong Fe and Mn signals observed during EDS analysis support the XRF and XRD findings, confirming the presence of Fe-Mn oxide mineralization. Silicon and aluminum signals indicate the existence of silicate gangue minerals, particularly quartz and aluminosilicate phases.

Elemental mapping analyses (Fig. 6) demonstrated that Fe, Mn, and O are broadly distributed across the sample surface and frequently overlap spatially. This overlapping distribution strongly suggests that iron, oxygen, and manganese coexist within mixed oxide phases such as bixbyite, as identified in XRD analysis. Manganese (Mn) exhibits a remarkably low tendency to form liberated individual grains.

Instead, Mn pixels are predominantly enclosed and finely disseminated as sub-micron inclusions within the Fe-oxide matrix, displaying a highly restrictive intimate intergrowth texture from a metallurgical standpoint.

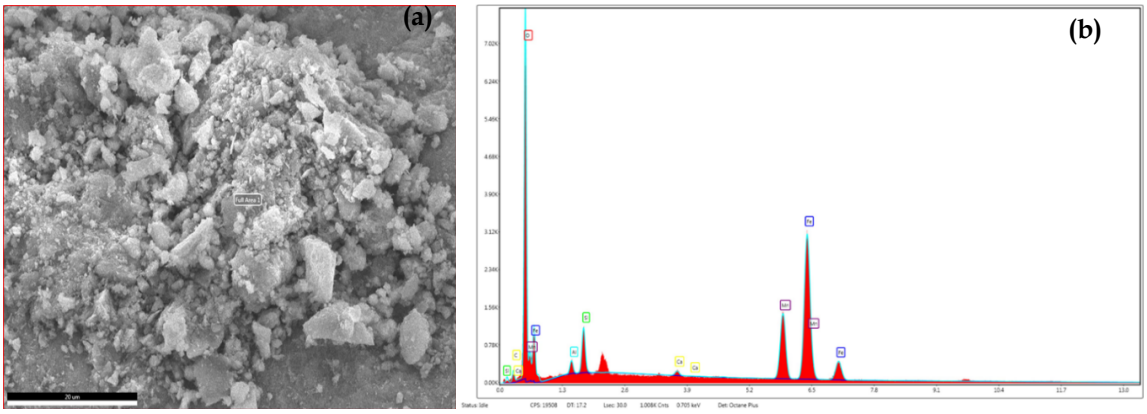

Fig. 5. SEM-EDS analysis of the ore sample: (a) SEM image (b) EDS spectrum

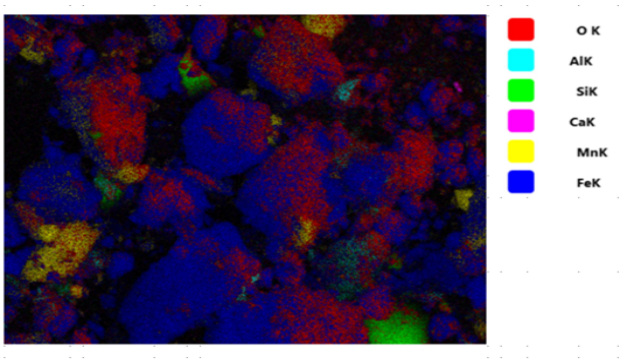

Fig. 6. SEM-EDS Elemental Mapping pattern of the ore sample

The close spatial association between Fe and Mn is mineralogically important because it may significantly influence beneficiation behavior. When Fe and Mn occur together within the same mineral structure, achieving selective separation becomes considerably more difficult. Consequently, advanced beneficiation techniques or selective chemical treatments may be required to enrich manganese efficiently.

The elemental distribution patterns additionally indicate that quartz-rich regions (Si-bearing gangue minerals; SiO_2) are relatively distinct from Fe-Mn-rich zones. They segregate into distinct, coarse, independent quartz (SiO_2) grains in specific zones (e.g., the bottom-right quadrant). This observation may be beneficial from a beneficiation perspective because quartz gangue minerals could potentially be separated through physical processing methods after sufficient liberation (Mehdilo et al., 2013).

The relatively homogeneous distribution of Fe and Mn throughout the investigated regions suggests that the ore does not contain highly localized manganese enrichment zones at the analyzed scale. Instead, the mineralization appears to be relatively disseminated within the oxide matrix.

As mentioned before, elemental mapping revealed the spatial distribution of Fe, Mn, Si, and O throughout the analyzed regions and suggested a close association between Fe- and Mn-bearing minerals. However, elemental mapping represents surface elemental distribution only and should not be interpreted as direct evidence of crystal-scale intergrowth or solid-solution relationships, because EDS-based mapping is constrained by X-ray excitation volume, spectral overlap, and phase-mixing effects that can obscure fine intergrowths (Georget et al., 2024). Quantitative process mineralogical techniques such as Mineral Liberation Analysis (MLA) or QEMSCAN provide more reliable information regarding mineral liberation, intergrowth characteristics, and phase associations (Gu et al., 2014). These analyses were beyond the scope of the present study and are recommended for future investigations aimed at strengthening beneficiation-oriented interpretation of the ore (Gu et al., 2014).

The combined SEM-EDS and mapping results demonstrate that the ore exhibits a complex intergrowth texture involving Fe-Mn oxide phases and siliceous gangue minerals. Such textural relationships are characteristic of many sub/low-grade ferruginous manganese deposits worldwide.

Moreover, the combined interpretation of XRF, XRD, and SEM–EDS analyses provides a more comprehensive understanding of the occurrence and mineralogical distribution of the major elements within the investigated ore. XRD-based phase identification in comparable manganoferrous (Fe–Mn) and sub/low-grade manganese ores consistently resolves goethite, Fe–Mn oxide phases including bixbyite/Fe-bearing bixbyite, and quartz/silica among the principal constituents. The available evidence supports interpreting iron as predominantly hosted in goethite and associated Fe-bearing oxide phases, because goethite is repeatedly identified as a major iron-bearing mineral and bixbyite is reported as a mixed $(Mn, Fe)_2O_3$ phase. The interpretation that manganese mainly occurs within the bixbyite phase is directly supported by studies identifying manganese in ferruginous manganese ore chiefly as oxide hosted in $(Mn, Fe)_2O_3$ (bixbyite), with bixbyite also listed among the significant Mn-bearing phases in ferruginous ores (Yi et al., 2017; Baioumy et al., 2013; Bhoja et al., 2021).

3.5. FT-IR analysis

FT-IR analysis was additionally conducted in order to investigate further the functional groups, lattice vibrations, hydroxyl-bearing phases, and silicate structures present within the investigated Fe-Mn oxide ore (Xiao et al., 2017). To the authors' knowledge, no paper has specifically analyzed low-grade manganoferrous (Fe-Mn) ores (%5-10 Mn) with bixbyite. The obtained FT-IR spectrum (Fig. 7) revealed several characteristic absorption bands associated with iron oxyhydroxides, manganese oxides, and silicate gangue minerals.

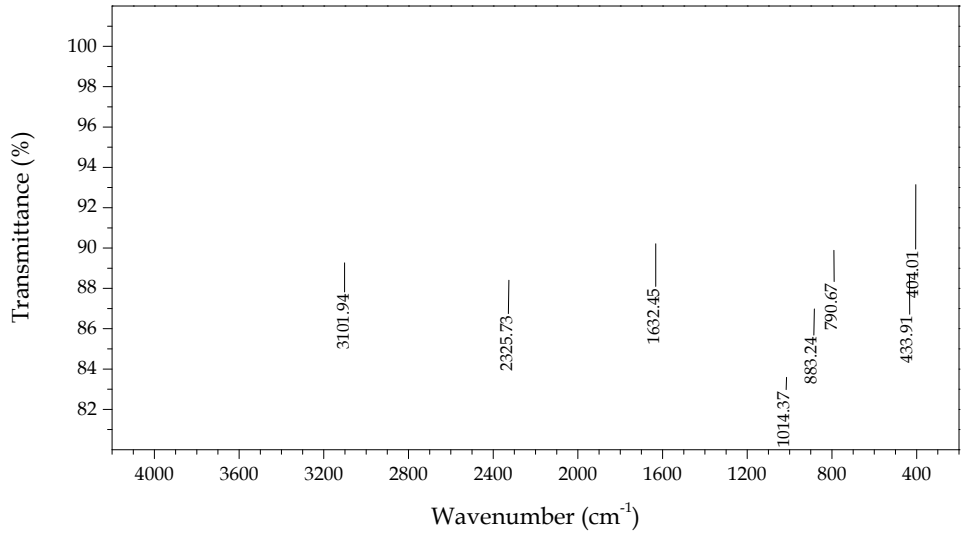

Fig. 7. FT-IR spectrum of the ore sample (ATR method)

The broad absorption region centered around approximately 3101 cm^{-1} is attributed to O–H stretching vibrations associated with structurally bonded hydroxyl groups and adsorbed water molecules. This absorption behavior strongly suggests the presence of hydroxyl-bearing iron minerals such as goethite [FeO(OH)] and secondary hydrated oxide phases. Similar hydroxyl-related absorption bands within the 3150–3450 cm^{-1} region were previously reported for goethite-rich systems by Ruan et al. (2002) and Prasad et al. (2006), who associated these vibrations with hydroxyl deformation and dehydroxylation characteristics of iron oxyhydroxides. The absorption band observed near 1632 cm^{-1} is attributed to H–O–H bending vibrations of adsorbed molecular water and hydroxylated mineral surfaces. Such bands are commonly observed in weathered ferruginous ore systems containing hydrated oxide minerals. Vázquez-Olmos et al. (2005) and Farghaly et al. (2020) reported Water OH bands near 3423 cm^{-1} and 1630 cm^{-1} for hydroxylated samples of pure synthetic Mn_3O_4.

In addition, the weak absorption feature around 2325 cm^{-1} is likely related to atmospheric CO_2 adsorption and/or minor carbonate-related surface species frequently encountered in oxide-rich mineral assemblages.

A strong absorption band centered near 1014 cm^{-1} corresponds to Si–O stretching vibrations, indicating the presence of quartz and silicate gangue minerals within the ore matrix. Similar quartz-related FT-IR absorptions between 1000 and 1100 cm^{-1} have been widely reported in ferruginous manganese ores and siliceous iron formations (Pani et al., 2016; Farghaly et al., 2020). These findings are fully consistent with the XRD results, where quartz was identified as one of the dominant mineral phases.

The fingerprint region of the FT-IR spectrum further confirms the coexistence of Fe- and Mn-bearing oxide phases. The absorption bands located at approximately 883 cm^{-1} and 790 cm^{-1} are assigned to Fe–OH bending and Fe–O lattice vibrations associated with goethite and related iron oxyhydroxide minerals. Previous FT-IR investigations on natural and synthetic goethite systems reported similar absorption features around 890 and 800 cm^{-1}, which are considered diagnostic bands for goethite-bearing mineral assemblages (Ruan et al. 2002; Pani et al. 2016).

Furthermore, the low-wavenumber absorption bands observed near 433 cm^{-1} and 404 cm^{-1} are attributed to Fe–O and Mn–O lattice vibrations originating from iron oxide and manganese oxide phases such as bixbyite and mixed Fe-Mn oxides. These low-frequency vibrations strongly support the coexistence of mixed Fe-Mn oxide structures previously identified by XRD analysis.

Overall, the FT-IR spectrum confirms that the investigated ore sample consists predominantly of hydroxyl-bearing iron oxides/oxyhydroxides, mixed Fe-Mn oxide phases, and quartz-rich silicate gangue minerals. The coexistence of hydroxyl bands together with Fe–O and Mn–O lattice vibrations further suggests that the ore may have undergone secondary oxidation, weathering, and hydrothermal alteration processes during mineralization. Consequently, the FT-IR findings strongly support the integrated mineralogical interpretation obtained from XRD, XRF, and SEM-EDS analyses and further demonstrate the heterogeneous oxide-silicate nature of the investigated Şırnak Fe-Mn ore.

The FT-IR interpretation presented in this study was conducted in conjunction with the XRD mineralogical results to improve the reliability of phase identification, since combined FT-IR/XRD approaches are widely used for mineral characterization and XRD can help resolve ambiguities arising from spectral disagreement or impurity-related complexity in infrared data (Makreski et al., 2004). This caution is particularly important for iron and manganese oxides, because multiple oxide minerals show absorption features in similar spectral regions, and manganese oxide spectra can vary substantially with structural disorder and hydration state (Potter and Rossman, 1979). Therefore, the assignment of individual absorption bands should be regarded as complementary support for mineral identification rather than independent proof of specific phases (Namduri and Nasrazadani, 2008).

3.6. TG-DTA-DTG thermal analysis

Thermogravimetric (TG), differential thermal (DTA), and derivative thermogravimetric analysis (DTG) investigations were performed in order to evaluate the thermal stability, dehydration behavior, phase transformation characteristics, and possible decomposition reactions of the investigated Fe-Mn oxide ore. The TG-DTA-DTG results revealed a multi-stage thermal decomposition behavior, which is typical for ferruginous manganese oxide systems containing hydroxyl-bearing iron phases and silicate gangue minerals (Fig. 8).

The TG curve exhibited a gradual mass loss throughout the heating process, with a significant weight reduction occurring mainly between approximately 200 °C and 350 °C. The total mass loss observed during this stage was approximately 11.9 wt.%, indicating substantial dehydration and dehydroxylation reactions within the ore matrix. This thermal behavior is strongly associated with the decomposition of hydroxyl-bearing iron minerals such as goethite (FeO(OH)) to hematite and the removal of structurally bound water molecules. Many researchers previously reported similar thermal decomposition characteristics for goethite-rich ferruginous systems (Alvarez et al., 2006; Salama et al., 2015; Rzepa et al., 2016), who demonstrated that goethite undergoes progressive dehydroxylation and transformation into hematite between 250 °C and 350 °C. The endothermic thermal effect observed

within this temperature interval further supports the dehydration and dehydroxylation behavior of hydrated iron oxide phases.

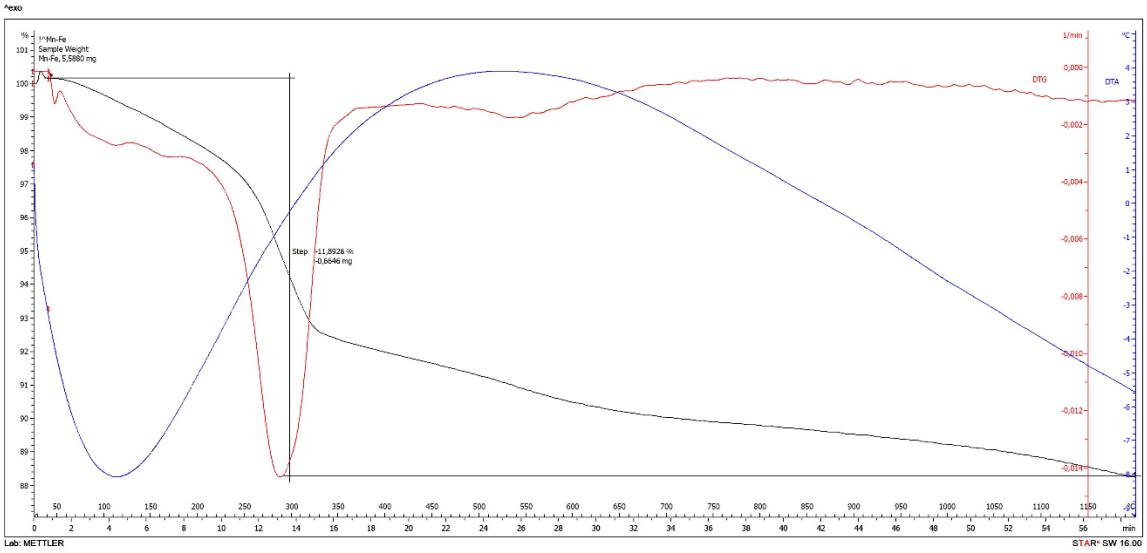

Fig. 8. TG- DTA-DTG curves of the ore sample

The DTA profile (Fig. 8) additionally revealed complex thermal reactions associated with phase transformation processes involving Fe-Mn oxide minerals. The broad thermal event observed between approximately 300 °C and 700 °C may indicate structural rearrangement and recrystallization of mixed Fe-Mn oxide phases such as bixbyite and secondary iron oxides. Similar thermal reactions have been reported in ferruginous manganese ores where manganese oxide phases exhibit partial structural transformation under elevated temperature conditions (Salama et al., 2015; Rzepa et al., 2016). Furthermore, the relatively smooth TG profile observed above approximately 700 °C suggests that the investigated ore possesses comparatively stable oxide phases at higher temperatures. At the same time, the absence of extremely sharp decomposition peaks indicates limited carbonate mineral content within the sample.

The derivative thermogravimetric (DTG) curve exhibited a pronounced mass-loss rate maximum at approximately 290 °C, corresponding to the major weight-loss event observed in the TG curve. This thermal event is attributed primarily to the dehydroxylation of goethite (FeO(OH)) and the associated transformation into hematite, accompanied by the release of structurally bound water (Ruan et al., 2001; Ruan et al., 2002; Frost et al., 2003). Beyond this temperature, the DTG signal gradually approached the baseline without distinct secondary peaks, indicating that the remaining mass loss occurred over a broad temperature interval and was associated with slow structural rearrangements and minor decomposition reactions rather than discrete thermal events. The absence of additional sharp DTG peaks is consistent with the predominance of thermally stable oxide phases such as bixbyite and quartz identified by XRD. Overall, the DTG profile supports the TG–DTA interpretation and confirms that the principal thermal transformation of the investigated Fe–Mn oxide ore occurs below 350 °C. In contrast, the mineral assemblage remains comparatively stable at higher temperatures (O'Hara et al., 2025).

The thermal behavior observed in the present study is also highly consistent with the mineralogical results obtained from XRD and FT-IR analyses. The presence of hydroxyl-related FT-IR bands together with the observed thermal mass loss strongly confirms the occurrence of hydrated iron oxyhydroxides such as goethite within the investigated ore system. Moreover, the gradual thermal decomposition profile suggests a heterogeneous oxide-silicate mineral assemblage rather than a single dominant mineral phase.

From a beneficiation and metallurgical perspective, the TG-DTA-DTG findings are particularly important because thermal decomposition characteristics directly influence roasting efficiency, magnetic phase transformation, and reduction behavior during pyrometallurgical processing of manganoferrous (Fe-Mn) ores. Previous studies demonstrated that controlled thermal treatment may significantly improve Fe/Mn separation efficiency through selective reduction and magnetic

transformation processes (Zhang and Cheng, 2007). Therefore, the obtained TG-DTA-DTG results provide valuable preliminary information for future reduction roasting, magnetic separation, and thermal beneficiation investigations involving the investigated Şırnak Fe-Mn oxide ore.

3.7. Crystalline size analysis

In order to further investigate the crystallographic characteristics of the investigated Fe-Mn oxide ore, crystallite size estimations based on the Scherrer equation (Eq. 1) were calculated. The Scherrer equation (Eq. 1) was applied to the major diffraction peaks in order to estimate average crystallite sizes of the identified mineral phases. The most characteristic and distinct peaks of quartz, goethite, and bixbyite were 26.68°, 21.28°, and 50.20°, respectively. According to the XRD raw data, the peak width at half maximum (FWHM) of quartz, goethite, and bixbyite were 0.156° (0.00272 rad.), 0.68° (0.01186 rad.), and 0.42° (0.00733 rad.), respectively. Based on calculations using the Scherrer formula (Eq. 1), the approximate crystal grain sizes of the quartz, goethite, and bixbyite phases were determined to be 548 Å (54.8 nm), 124 Å (12.4 nm), and 206.3 Å (20.6 nm), respectively.

Applying the Scherrer equation to the prominent reflection of goethite at 2-theta of 21.28° (FWHM = 0.68°) yields an average crystallite size of 12.4 nm (125 Å). This ultra-fine nanomaterial scale accounts for the poorly crystalline, porous framework that was previously shown to drive a substantial 11.89 wt.% mass loss via rapid dehydroxylation in the intermediate TG-DTG thermal window.
The evaluation of the bixbyite phase across its diagnostic Bragg reflection at 33.14° (FWHM = 0.42°) indicates a structural crystallite size of 20.6 nm (206 Å). This intermediate crystallinity profile underpins the high-temperature stability of the ore.

In the case of quartz, the sharpest diffraction peak at 2-theta of 26.689° exhibits a remarkably narrow full-width at half-maximum (FWHM = 0.156°), translating into a significantly larger crystallite size of 54.8 nm (548 Å) via Scherrer calculation. The dual presence of large quartz crystallites alongside nanometer-scale iron-manganese oxide particles explains the thermodynamic masking observed during prior differential thermal tests. At the same time, the quartz phase exhibits high crystallinity-consistent with the intense Si-O-Si stretching signals at 1014.37 cm^{-1} in the FTIR spectra.

The integrated mineralogical characterization performed in this study provides important preliminary information for evaluating potential beneficiation strategies for the investigated Fe–Mn oxide ore. The coexistence of goethite, bixbyite, and quartz suggests that the efficiency of subsequent magnetic separation, reduction roasting, or hydrometallurgical processing may be strongly influenced by the mineral assemblage and the spatial association of Fe- and Mn-bearing phases (Baioumy et al., 2013; Cheraghi et al., 2020; Niyonzima et al., 2021). Although beneficiation experiments were beyond the scope of the present investigation, the comprehensive characterization dataset establishes a reliable mineralogical basis for selecting and optimizing future processing routes.

4. Conclusions

Compared with high-grade manganese ores, the investigated sample contains relatively lower manganese concentrations and higher iron and silica contents. Nevertheless, the existence of economically relevant Mn concentrations together with mixed Fe-Mn oxide phases makes the ore scientifically valuable and potentially suitable for future beneficiation studies. The identification of bixbyite is particularly important because this mineral may serve as an indicator of complex hydrothermal or supergene mineralization processes. Furthermore, bixbyite-bearing ores may exhibit unique beneficiation characteristics due to the intimate association between Fe and Mn within the crystal structure.

Despite the existence of several studies concerning ferruginous manganese mineralization in Türkiye, China, and India (Table 2), detailed integrated characterization studies specifically focusing on Fe-Mn oxide systems from the Şırnak region remain relatively limited in the available literature. In particular, to the authors' knowledge, combined XRD-XRF-SEM/EDS-FT-IR, TG-DTA-DTG investigations addressing natural bixbyite-bearing ferruginous manganese ores (including ores from southeastern Türkiye) do not exist. Therefore, the present study contributes to the limited mineralogical database of southeastern Türkiye Fe-Mn deposits by providing integrated mineralogical, chemical, and microstructural characterization data. The obtained findings may serve as preliminary reference data

for future liberation analysis, beneficiation optimization, reduction roasting, magnetic separation, and hydrometallurgical extraction studies involving similar ferruginous manganese ore systems.

Furthermore, the identification of mixed Fe-Mn oxide phases such as bixbyite provides valuable insight into the mineralogical complexity and potential beneficiation behavior of the investigated ore. The strong association between Fe and Mn phases observed through XRD and elemental mapping analyses suggests that selective separation may require advanced beneficiation approaches.

Table 2. Comparison of selected studies reported in literature and the investigated Şırnak (Fe-Mn) ore

Location	Mn (%)	Fe (%)	Main Minerals	Gangue Minerals	Characterization Methods	Reference
Elazığ–Malatya, Türkiye	11–30	Variable	Braunite, bixbyite, Pyrolusite	Quartz, barite, pyrite	XRD, Optical microscopy, SEM, ICP (major and trace elements)	(Şaşmaz et al., 2014)
Battalgazi–Malatya, Türkiye	18.15 (average: 23.44% MnO)	30.2 (average: %43.25 Fe_2O_3)	Psilomelane, Hematite, limonite, Bixbyite	Clay, quartz	XRD, Chemical analysis, microscopy	(Yapici and Bahçeli, 2012)
Ceyhan-Adana-Türkiye	15.03	25.04	Hematite, Goethite, Manganite, Maghemite, Ramsdellite	Quartz, calcite, garnet	XRD-AAS	(Top et al., 2022)
Tabriz, Iran	13.8% MnO	-	Pyrolusite	Quartz, Calcite	XRD, XRF, SEM-WDX, Optical microscopy	(Mehdilo et al., 2013)
Zhomart, Kazakhstan	15.8% of braunite $(Mn_2O_3)_3 \cdot MnSiO_3$, and 9.6% of MnO_2	24.3	Hematite, Braunite, Pyrolusite	Silicate, Calcite	XRD, Polarized light microscopy	(Dyussenova et al., 2024)
India	30.83	24.28	Goethite, pyrolusite	Silicates	XRD, Chemical analysis, SEM	(Reddy et al., 2019)
China	35.26	21.28	Bixbyite, hematite	Quartz	XRD, SEM-EDS	(Yi et al., 2017)
Şırnak, Türkiye (Present Study)	9.77	29.7	Bixbyite, goethite	Quartz	XRD, XRF, SEM-EDS, Elemental Mapping, FT-IR, TG-DTA-DTG.	Present study

To conclude, XRD analysis identified quartz, goethite, and bixbyite as the major mineral phases constituting the investigated Fe–Mn oxide ore. XRF results revealed that the ore is characterized by high iron content, moderate manganese concentration, and significant silica content, confirming its classification as manganoferrous (Fe-Mn) ore or low/sub-grade ferruginous manganese ore. SEM–EDS and elemental mapping analyses demonstrated a heterogeneous mineral distribution and a close spatial association between Fe- and Mn-bearing phases, indicating complex mineral intergrowths within the ore matrix.

FT-IR analysis confirmed the presence of hydroxyl-bearing iron oxyhydroxides, mixed Fe–Mn oxide phases, and quartz-rich silicate gangue through characteristic O–H, Fe–O, Mn–O, and Si–O vibrational bands. TG-DTA results revealed multi-stage thermal decomposition behavior with an overall mass loss associated mainly with dehydration and dehydroxylation reactions of goethite-bearing phases. These findings provided valuable information regarding the thermal stability and phase transformation characteristics of the ore.

Overall, the combined XRD, XRF, SEM–EDS, elemental mapping, FT-IR, and TG-DTA-DTG results demonstrated that the investigated Şırnak Fe–Mn ore consists of a complex oxide–silicate mineral assemblage characterized by heterogeneous microstructures and intimate Fe–Mn associations. The integrated characterization approach provides a comprehensive mineralogical and physicochemical database that may support the design and optimization of future beneficiation and metallurgical processing studies of similar Fe–Mn oxide ores.

Acknowledgments

The authors would like to thank Mr. Şahin Ölgen for providing the samples used in this study.

A part of the results reported in this paper were presented at XX Balkan Mineral Processing Congress BMPC2026 entitled "Characterization of manganoferrous (Fe-Mn) oxide ore from Türkiye-Şırnak region".

References

ALI, H., EL-SADEK, M., AHMED, H., 2023. *Investigation of transformations of low-grade manganese ore during the roasting process*. Miner. Process. Extr. Metall. 132 (1): 62–72.

ALI, S., IQBAL, Y., FAROOQ, U., AHMAD, S., 2016. *Leaching of manganese ores using corncob as reductant in H_2SO_4 solution*. Physicochem. Probl. Miner. Process. 52, 1, 56–65.

ALVAREZ, M., RUEDA, E.H., SILEO, E.E., 2006. *Structural characterization and chemical reactivity of synthetic Mn-goethites and hematites*. Chem. Geol. 231 (4): 288–299.

BAIOUMY, H.M., KHEDR, M.Z., AHMED, A.H., 2013. *Mineralogy, geochemistry and origin of Mn in the high-Mn iron ores, Bahariya Oasis, Egypt*. Ore Geol. Rev. 53: 63–76.

BHOJA, S.K., TRIPATHY, S.K., MURTHY, Y.R., GHOSH, T.K., KUMAR, C.R., CHAKRABORTY, D.P., 2021. *Influence of Mineralogy on the Dry Magnetic Separation of Ferruginous Manganese Ore – A Comparative Study*. Minerals. 11 (2): 150.

BOZTAS, S., ATAKOGLU, O.O. YALCIN, M.G. 2025. T*he Origin and Geochemistry of the Kumluca Manganese Deposit in the South West, Antalya Province, Türkiye: Possibility of Derived Hydrothermal Fluids*. Min. Metall. Explor. 42 (5): 3161–3193.

ÇARDAKLI, I.S., 2010. *Production of High Carbon Ferromanganese from A Manganese Ore Located in Erzincan*.MSc. Thesis, Middle East Technical University, Ankara, Türkiye, 66pp.

CHERAGHI, A., BECKER, H., EFTEKHARI, H., YOOZBASHIZADEH, H., SAFARIAN, J., 2020. *Characterization and calcination behavior of a low-grade manganese ore*. Mater. Today Commun. 25: 101382.

CHRISTIE, T., 2007. *Mineral Commodity Report 7 – Manganese*. New Zealand, Institute of Geological and Nuclear Sciences Ltd.

CULLITY, B.D., 1956. *Elements of X-Ray Diffraction*. In Addison-Wesley Series in Metallurgy and Materials. Addison- Wesley, Reading, Massachusetts.

DYUSSENOVA, S., LUKHMENOV, A., IMEKESHOVA, M., AKIMZHANOV, Z.A., 2024. *Investigation of the beneficiation of refractory ferromanganese ores "Zhomart" deposits*. Complex Use of Mineral Resources, 329, 2, 34–42.

ELMI, C., WHITLOCK, J.R., MACDOWELL, M.T., FOUST, R.D., 2023. *Insights on the Formation Conditions of Manganese Oxides from Crimora, VA (USA)*. Geosci. 13 (8): 235.

FARGHALY, M., ABDEL-KHALEK, N., ABDEL-KHALEK, M., SELIM, K., ABDULLAH, S., 2020. *Physicochemical study and application for pyrolusite separation from high manganese-iron ore in the presence of microorganisms*. Physicochem. Probl. Miner. Process. 57, 1, 273–284.

FROST, R.L., DING, Z., RUAN, H., 2003. *Thermal Analysis of Goethite - Relevance to Australian Indigenous Art*. J. Therm. Anal. Calorim. 71 (3): 783–797.

GAO, Y., OLIVAS-MARTINEZ, M., SOHN, H.Y., KIM, H.G., KIM, C.W., 2012. *Upgrading of Low-Grade Manganese Ore by Selective Reduction of Iron Oxide and Magnetic Separation*. Metall. Mater. Trans. B. 43 (6): 1465–1475.

GHADIRI, M., HARRISON, S. T., FAGAN-ENDRES, M. A., 2020. *Quantitative X-ray μCT measurement of the effect of ore characteristics on non-surface mineral grain leaching*. Minerals. 10(9), 746.

GEORGET, F., SCHMATZ, J., WELLMANN, E., MATSCHEI, T., 2024. A *critical catalogue of SEM-EDS multispectral maps analysis methods and their application to hydrated cementitious materials*. Journal of Microscopy 294: 105–116.

GU, Y., SCHOUWSTRA, R.P., RULE, C., 2014. *The value of automated mineralogy*. Miner. Eng. 58: 100–103.

IMAMOĞLU, M.Ş., 2005. *Evaluation of Southeastern Anatolia Region and Its Vicinity in Terms of Mineral Deposits.* Proceedings Book of the Symposium on Evaluation of Mineral Resources in Eastern and Southeastern Anatolia, 21-23 April 2005, Diyarbakır, Türkiye, 87–92 (in Turkish).

ISMAIL, S., HASHIM, S.F.S., HUSSIN, H., ABDULLAH, N.S., 2016. *Chemical and mineralogical characterization of Malaysian low-grade manganese ore*. Period. Mineral. 85, 277-288.

LI, H., XU, W., 2024. *Geological and Economic Assessment of Manganese Deposits.* Int. J. Ecol. Environ. Sci. 6, 2, 28–31.

LI, H., ZHANG, W., SUN, K., GUO, J., YUAN, K., FU, J., ZHANG, T., ZHANG, X., LONG, H., ZHANG, Z., LAI, Y., SUN, H., 2021. *Manganese-Based Materials for Rechargeable Batteries beyond Lithium-Ion*. Adv. Energy Mater. 11, 25, 2100867.

LIU, X., ZHAO, Y., ZHOU, W., YUAN, S., WANG, X., 2024. *New progress in the development and utilization of ferromanganese ore.* Miner. Eng. 216, 108826.

LOTTER, N.O., KORMOS, L.J., OLIVEIRA, J., FRAGOMENI, D., WHITEMAN, E., 2011. *Modern Process Mineralogy: Two case studies.* Miner. Eng. 24, 7, 638–650.

MAKRESKI, P., JOVANOVSKI, G., KAITNER, B., STAFILOV, T., BOEV, B., CIBREV, D., 2004. *Minerals from Macedonia. X. Separation and identification of some oxide minerals by FT-IR spectroscopy, AAS, AES-ICP and powder XRD*. Neues Jahrb. für Mineral. Abh 180 (3): 215–243.

MAYNARD, J.B., 1983. *Geochemistry of Sedimentary Ore Deposits*. Springer New York, New York, USA, 306 pp.

MEHDILO, A., IRANNAJAD, M., HOJJATI-RAD, M.R., 2013. *Characterization and beneficiation of Iranian low-grade manganese ore.* Physicochem. Probl. Miner. Process. 49, 3, 725–741.

MOUSTAFA, A., ABDEL-KHALEK, N., SHARAF-ELDIN, A., SOLTAN, A., HASSAN, E.S., 2024. *Beneficiation of Ferruginous Manganese Ore of Um Bogma Locality, Sinai: Comparison Between Conventional Reduction Roasting Techniques and Microwave Technology*. Rud.-geol.-naft. zb. 39, 5, 89–100.

NAMDURI, H., NASRAZADANI, S., 2008. *Quantitative analysis of iron oxides using Fourier transform infrared spectrophotometry.* Corros. Sci. 50 (9): 2493–2497.

NASERI, M., IRANNAJAD, M., MEHDILO, A., 2026. *Recent advances in the synthesis of manganese oxide nanoparticles and comparative evaluation of their biological activities*. Sustain. Chem. Clim. 9, 100216.

NIYONZIMA, J.C., LUO, L., EDO, E.E., MUSTAFA, S., 2021. *Mineralogical Characterization and Optimization of Fe and Mn Through Roast-Leaching of Ferromanganese Ore*. Min. Metall. Explor. 38, 3, 1509–1523.

O'HARA, R.L., COOK, N.J., LEWIS, E.W., ARJOMANDI, M., BROOKS, G., CHINNICI, A., 2025. *Thermally Assisted Beneficiation of a Low-Grade Iron Ore Powder in a Pilot-Scale Drop Tube Reactor: Effects on Ore Upgrading, Mineralogy and Chemical-Physical Characteristics.* Metall. Mater. Trans. B. 56 (6): 6348–6367.

ÖZTÜRK, H., KASAPÇI, C., ÖZBAŞ, F., 2019. *Manganese Deposits of Turkey. In*: Pirajno, F., Ünlü, T., Dönmez, C. , Şahin, M.B. (eds.), *Mineral Resources of Turkey*, Vol. 16, 261–281. Springer International Publishing, Cham.

PANI, S., SINGH, S.K., MOHAPATRA, B.K., 2016. *Vibrational Spectroscopic Study for Qualitative Assessment of Mn-oxide Ore*. Resour. Geol. 66, 1, 12–23.

POOJARI, M., VARDHAN, H., JATHANNA, H.M., 2024. *Iron Ore Characterization Techniques in Mineral Processing.* J. Inst. Eng. India. Ser. D. 105, 1, 543–551.

POTTER, R.M., ROSSMAN, G.R., 1979. *The tetravalent manganese oxides: identification, hydration, and structural relationships by infrared spectroscopy.* Am. Mineral. 64: 1199–1218.

PRASAD, P.S.R., SHIVA PRASAD, K., KRISHNA CHAITANYA, V., BABU, E.V.S.S.K., SREEDHAR, B., RAMANA MURTHY, S., 2006. *In situ FTIR study on the dehydration of natural goethite.* J. Asian Earth Sci. 27, 4, 503–511.

REDDY, U.M., GOPALKRISHNA, S.J., KUMAR, P.S., HATTI, B., 2019. *Characterization and Processing of Low Grade Iron Rich Manganese Ore*. Int. J. Sci. Technol. Res. 8, 12, 2448-51.

RINGDALEN, E., GJOVIK, J.E., LARSSEN, T.A., TANGSTAD, M., 2021. *Pretreatment of Manganese Ores in Different Gas-Atmospheres- a Method to Reduce Energy Consumption and CO_2 Emissions in Mn-Alloy Production.* Proceedings of the 16th international ferro-alloys congress (INFACON XVI): 1–12.

RUAN, H.D., FROST, R.L., KLOPROGGE, J.T., 2001. *The behavior of hydroxyl units of synthetic goethite and its dehydroxylated product hematite*. Spectrochim. Acta A Mol. Biomol. Spectrosc. 57 (13): 2575–2586.

RUAN, H.D., FROST, R.L., KLOPROGGE, J.T., DUONG, L., 2002. *Infrared spectroscopy of goethite dehydroxylation: III. FT-IR microscopy of in situ study of the thermal transformation of goethite to hematite.* Spectrochim. Acta A Mol. Biomol. Spectrosc. 58, 5, 967–981.

RZEPA, G., BAJDA, T., GAWEL, A., DEBIEC, K., DREWNIAK, L., 2016. *Mineral transformations and textural evolution during roasting of bog iron ores*. J. Therm. Anal. Calorim. 123, 1, 615–630.

SAFAROV, R.Z., BAIKENOV, Y.A., ZHANDILDENOVA, A.K., KOPISHEV, E.E., KAMATOV, R.M., KARGIN, J.B., SANCHEZ CORNEJO, H., BARNES, C.H.W., DE LOS SANTOS VALLADARES, L., 2025. *Phase Transitions and Structural Evolution of Manganese Ores During High-Temperature Treatment.* Metals, 15, 1, 89.

SALAMA, W., EL AREF, M., GAUPP, R., 2015. *Spectroscopic characterization of iron ores formed in different geological environments using FTIR, XPS, Mössbauer spectroscopy and thermoanalyses.* Spectrochim. Acta A Mol. Biomol. Spectrosc. 136, 1816–1826.

STATE PLANNING ORGANIZATION (DPT) (2001). *Mining special expertise commission report: Metal minerals sub-commission other metal minerals working group report - Antimony - Tungsten - Nickel - Vanadium - Molybdenum - Tin - Manganese* (Publication No: ÖİK 633). State Planning Organization (DPT), Türkiye, Ankara (in Turkish).

ŞAŞMAZ, A., TÜRKYILMAZ, B., ÖZTÜRK, N., YAVUZ, F., KUMRAL, M., 2014. *Geology and geochemistry of Middle Eocene Maden complex ferromanganese deposits from the Elazığ–Malatya region, Eastern Turkey*. Ore Geol. Rev. 56, 352–372.

SCHOUWSTRA, R.P., SMIT, A.J., 2011. *Developments in mineralogical techniques – What about mineralogists?* Miner. Eng. 24, 12, 1224–1228.

SEMSARI PARAPARI, P., PARIAN, M., ROSENKRANZ, J., 2022. *Quantitative analysis of ore texture breakage characteristics affected by loading mechanism: Fragmentation and mineral liberation*. Miner. Eng. 182, 107561.

SINGH, V., CHAKRABORTY, T., TRIPATHY, S.K., 2020. *A Review of Low Grade Manganese Ore Upgradation Processes*. Miner. Process. Extr. Metall. Rev. 41, 6, 417–438.

SOBOUTI, A., SHAFAAT, N., ABDOLLAHZADEH, A.A., 2020. *Jiroft refractory manganese ore leaching using oxalic acid as reducing agent in sulfuric acid solution*. Physicochem. Probl. Miner. Process. 56, 2, 373–384.

TOP, S., ALTINER, M., KURŞUNOĞLU, S., 2022. *Farklı indirgeyiciler kullanılarak bir manganlı demir cevherinden mangan çözündürülmesinin araştırılması.* Sci. Min. J. 61, 2, 83–92 (in Turkish).

U.S. GEOLOGICAL SURVEY. 2021. *Mineral Commodity Summaries 2021*. U.S. Geological Survey, 200 pp.

VÁZQUEZ-OLMOS, A., REDÓN, R., RODRÍGUEZ-GATTORNO, G., ESTHER MATA-ZAMORA, M., MORALES-LEAL, F., FERNÁNDEZ-OSORIO, A.L., SANIGER, J.M., 2005. *One-step synthesis of Mn_3O_4 nanoparticles: Structural and magnetic study*. J. Colloid Interface Sci. 291, 1, 175–180.

XIAO, J., HE, J., YANG, H., WU, C., XU, J., LI, Y., 2019. *Geochemical Characteristics and Genetic Significance of Datangpo-Type Manganese Ore Deposits during the Cryogenian Period.* Resour. Geol. 69, 3, 227–248.

XIAO, W., JONES, A.M., COLLINS, R.N., BLIGH, M.W., WAITE, T.D., 2017. *Use of Fourier transform infrared spectroscopy to examine the Fe(II)-Catalyzed transformation of ferrihydrite*. Talanta, 175, 30–37.

YAN, H., PI, D.H., JIANG, S.Y., MAO, J., XU, L., YANG, X., HAO, W., MÄND, K., LI, L., KONHAUSER, K.O., ROBBINS, L.J., 2022. *Mineral paragenesis in Paleozoic manganese ore deposits: Depositional versus post-depositional formation processes*. Geochim. Cosmochim. Acta. 325, 65–86.

YAPICI, N., BAHÇELI, A., 2012. *Battalgazi (Malatya) Bölgesi Manganez Cevherleşmelerinin Mineralojik, Jeokimyasal Özellikleri ve Zenginleştirilebilirliğinin Araştırılması.* Çukurova University Journal of the Faculty of Engineering and Architecture. 27, 2, 61–71. (in Turkish).

YI, L., HUANG, Z., JIANG, T., ZHAO, P., ZHONG, R., LIANG, Z., 2017. *Carbothermic Reduction of Ferruginous Manganese Ore for Mn/Fe Beneficiation: Morphology Evolution and Separation Characteristic*. Minerals. 7, 9, 167.

ZHANG, W., CHENG, C.Y., 2007. *Manganese metallurgy review. Part I: Leaching of ores/secondary materials and recovery of electrolytic/chemical manganese dioxide*. Hydrometallurgy. 89, 3, 137–159.